

Vertically-resolved observations of Jupiter’s quasi-quadrennial oscillation from 2012 to 2019

R. S. Giles^{a,*}, T. K. Greathouse^a, R. G. Cosentino^{b,c}, G. S. Orton^d, J. H. Lacy^e

^aSouthwest Research Institute, San Antonio, TX, USA

^bNASA Goddard Spaceflight Center, Greenbelt, MD, USA

^cCRESST II and Department of Astronomy, University of Maryland, College Park, MD, USA

^dJet Propulsion Laboratory / California Institute of Technology, Pasadena, CA, USA

^eUniversity of Texas at Austin, Austin, TX, USA

Abstract

Over the last eight years, a rich dataset of mid-infrared CH₄ observations from the TEXES instrument at IRTF has been used to characterize the thermal evolution of Jupiter’s stratosphere. These data were used to produce vertically-resolved temperature maps between latitudes of 50°S and 50°N, allowing us to track approximately two periods of Jupiter’s quasi-quadrennial oscillation (QQO). During the first five years of observations, the QQO has a smooth sinusoidal pattern with a period of 4.0 ± 0.2 years and an amplitude of 7 ± 1 K at 13.5 mbar (our region of maximum sensitivity). In 2017, we note an abrupt change to this pattern, with the phase being shifted backwards by ~ 1 year. Searching for possible causes of this QQO delay, we investigated the TEXES zonally-resolved temperature retrievals and found that in May/June 2017, there was an unusually warm thermal anomaly located at a latitude of 28°N and a pressure of 1.2 mbar, moving westward with a velocity of 19 ± 4 ms⁻¹. We suggest that there may be a link between these two events.

Keywords: Jupiter; Atmospheres, structure; Infrared observations; Spectroscopy

1. Introduction

Long-term observations of Jupiter have shown periodic variations in the planet’s stratospheric temperatures. Between 1980 and 2001, 7.8- μ m images of Jupiter from NASA’s Infrared Telescope Facility (IRTF) were used to track the brightness temperature of Jupiter’s atmosphere in the 10–20 mbar region (Orton et al., 1991; Leovy et al., 1991; Friedson, 1999; Simon-Miller et al., 2006). These observations showed an oscillation in the equatorial and low-latitude regions of the planet with a period of ~ 4 years; the stratospheric temperatures oscillate between having a local maximum at the equator and local minima at planetocentric latitudes of $\pm 13^\circ$, and having a local minimum at the equator and local maxima at planetocentric latitudes of $\pm 13^\circ$. This phenomenon was named the quasi-quadrennial oscillation (QQO) by Leovy et al. (1991), who noted its resemblance to the quasi-biennial oscillation (QBO) that is seen in the Earth’s stratosphere.

The QBO is a quasi-periodic oscillation in the Earth’s stratospheric zonal mean winds at tropical latitudes (Baldwin et al., 2001). At a given pressure level, the equatorial wind direction oscillates between easterly and westerly with a mean period of 28 months. The easterly and westerly wind regimes propagate downwards with time,

so there is a phase offset between different pressure levels and a vertical wind shear that alternates between positive and negative. On both Earth and Jupiter, the mean zonal flow can be assumed to be in approximately hydrostatic and geostrophic balance (Leovy et al., 1991), which means that the vertical wind shear and the horizontal temperature gradient are coupled through the thermal wind equation (Baldwin et al., 2001). Unlike on the Earth, it is difficult to make direct wind measurements in Jupiter’s stratosphere, but it is possible to study the QQO’s signature and evolution by observing changes in the temperature field.

Despite being an equatorial phenomenon, the QBO has a significant impact on the dynamics of the Earth’s atmosphere at all latitudes; this includes affecting the strength of Atlantic hurricanes and the breakdown of the winter-time stratospheric polar vortices (Baldwin et al., 2001). The QQO may also be an important factor in Jupiter’s weather patterns, and close monitoring of the QQO phase pattern is required to make any correlations with observed dynamical changes. Careful analysis of the QQO also provides insight into the waves that are thought to drive the phenomenon. The Earth’s QBO is driven by the absorption of vertically-propagating atmospheric waves that break and deposit their zonal momentum at a critical level that is determined by the background zonal flow (Baldwin et al., 2001). For the Earth, Dunkerton (1997) showed that a combination of Kelvin, Rossby-gravity, inertia-gravity,

*Corresponding author

Email address: rgiles@swri.edu (R. S. Giles)

and smaller-scale gravity waves are required to reproduce observed winds and temperatures. Similar mechanisms have been proposed as the driving forces behind Jupiter’s QGO, and observations play an important role in constraining atmospheric models.

The first models of the QGO were developed by Friedson (1999) and Li and Read (2000), who were both able to reproduce QGO-like phenomena within mechanistic models of Jupiter’s atmosphere; Li and Read (2000) suggested that equatorial oscillations could be produced using a combination of planetary-scale waves, while Friedson (1999) implemented a flat-spectrum gravity wave drag parameterization and compared the effects of gravity waves and planetary-scale waves, finding that small-scale, short-period gravity were better able to drive a QGO-like phenomenon. However, these studies were limited by the observations that were available at the time. The 7.8- μm broad-band imaging campaign provided a valuable dataset over a long timeframe, but was limited to a single pressure range and did not have any sensitivity to vertical variations in the thermal profile.

More recent studies of Jupiter’s QGO have made use of spacecraft data from Voyager IRIS (Simon-Miller et al., 2006) and Cassini CIRS (Flasar et al., 2004; Simon-Miller et al., 2006). Both of these instruments provide spectroscopic observations of Jupiter, allowing vertical temperature profiles to be retrieved in the stratosphere. This vertical information is an important addition to the studies of the QGO, but as the spacecraft observations were obtained during flybys of Jupiter, they were each restricted to short timeframes and cannot be used to study how the QGO varies with time.

In order to improve our three-dimensional understanding of the QGO and to inform future modeling efforts, we began a long-term study of Jupiter’s stratospheric temperatures in 2012, using the Texas Echelon Cross Echelle Spectrograph (TEXES, Lacy et al., 2002), which operates as a visitor instrument at the IRTF. TEXES provides high-resolution ($R=80,000$) spectroscopy of line profiles, which allows us to vertically resolve the temperature structure in Jupiter’s stratosphere to a greater degree than was possible with the lower resolution Voyager IRIS and Cassini CIRS observations. After the first complete cycle was observed (2012–2016), the data were used to constrain a new General Circulation Model (GCM) analysis by Cosentino et al. (2017). The TEXES observations showed that the QGO extends upwards to lower pressures (~ 2 mbar) than previously known, and that there is a smooth sinusoidal transition between maxima and minima over a large range of pressures. Cosentino et al. (2017) concluded that high-frequency gravity waves are significant contributors of momentum to the QGO, agreeing with earlier results from Friedson (1999). In particular, Cosentino et al. (2017) found that a stochastic gravity wave drag parameterization, representative of an atmosphere with convection, is better able to model the observations.

We have now been observing Jupiter’s QGO with

TEXES/IRTF for approximately eight years, which corresponds to two cycles. These data allow us to look for additional variability superimposed on top of the QGO. In 2015–16, an unusual disruption to the Earth’s QBO was noted by Osprey et al. (2016) and Newman et al. (2016). The exact causes of this event are still unclear, but both studies suggest it may be due to intrusion of Rossby waves from the winter hemisphere into the equatorial region of the planet. Like Jupiter, Saturn also has an oscillation in the equatorial stratosphere, known as Saturn’s Semi-Annual Oscillation (SSAO), and this has been observed to be disrupted by a large long-lasting storm in the northern mid-latitudes (Fletcher et al., 2017a).

In this paper, we present an updated vertically resolved time series of Jupiter’s QGO covering the 2012–2019 time period. We find that after five years of smoothly varying sinusoidal behaviour, there was a change in the QGO behaviour in 2017, and we use our spatially resolved observations to show that this occurred in conjunction with a localized stratospheric thermal anomaly. The TEXES observations and the data reduction process are described in Section 2 and the radiative transfer model is presented in Section 3. The long-term QGO observations and the 2017 disruption are discussed in Section 4 and the conclusions are summarized in Section 5.

2. Observations

2.1. TEXES observations

Between 2012 and 2019, high-resolution mid-infrared observations of Jupiter were made with the TEXES instrument, mounted at the 3-m NASA Infrared Telescope Facility. Data were obtained during eighteen observing runs, summarized in Table 1. TEXES is a cross-dispersed grating spectrograph that covers wavelengths of 4.5–25 μm in the mid-infrared, with a resolving power between 4,000 and 80,000 depending on the mode of operation. The scan-map mode of TEXES produces spectral datacubes (two spatial dimensions and one spectral dimension) of extended objects by stepping the slit across the sky perpendicular to the slit length.

In order to study Jupiter’s stratospheric temperatures, we used observations centered at 1247.5 cm^{-1} (8.02 μm), with a spectral bandpass of ~ 7 cm^{-1} . This spectral range covers six strong P-branch lines of the CH_4 ν_4 band, which is centered at 1306 cm^{-1} (Brown et al., 2003). TEXES was used in its highest spectral resolution mode ($R=80,000$), which means that these lines are spectrally resolved. CH_4 is homogeneously mixed in Jupiter’s stratosphere, and its abundance is well known. Variations in the shapes of CH_4 emission lines are due to temperature variations alone and these emission lines therefore provide a direct measurement of Jupiter’s stratospheric temperature. At the center of the strong emission lines, the atmosphere becomes optically thick at high altitudes in the stratosphere, so we are sensitive to temperatures at those high altitudes. In the

wings of those strong lines, or in the center of weaker lines, the atmosphere does not become opaque until a lower altitude, and so we can probe deeper into the stratosphere. By simultaneously modeling the 1244–1251 cm^{-1} spectral range, we are able to retrieve the vertical temperature profile in the 0.1–30 mbar pressure region.

Three-dimensional temperature maps covering the 50°S – 50°N latitude range were built up by using the TEXES scan-map mode. We oriented the slit along the celestial north-south direction and scanned across the planet from west to east. We used a step size of $0.7''$ (half the width of the slit) and observations of sky were included at the beginning and end of each scan to aid with sky subtraction. In the high-resolution observing mode, the TEXES slit length is $6''$, which is considerably smaller than the diameter of Jupiter (see Table 1). In order to cover the entire 50°S – 50°N latitude range, we therefore performed multiple scans with different north-south offsets. This observing sequence was repeated continuously for ~ 6 hours on a single night; due to Jupiter’s rotation period of 10 hours, this provides coverage of over half of the planet. When possible, observations on a subsequent night were then used to complete the global map. Table 1 shows that we were able to obtain full longitudinal coverage at the equator on the vast majority of the observing runs.

At 1247.5 cm^{-1} , the diffraction limit at the 3-m IRTF is $0.7''$, which is comparable to the typical seeing at the telescope. For the angular diameters provided in Table 1, this is equivalent to a spatial resolution of $\sim 2^\circ$ latitude at the equator. In the longitudinal direction, the $1.4''$ slit width leads to a spatial resolution of $\sim 4^\circ$ longitude.

Our long-term observing program was designed to study both long- and short-term variability in Jupiter’s stratospheric temperatures. In order to track the long-term trends in temperature, observations were made on several observing runs per year. These runs were nominally planned as pairs with a 1-month spacing about each quadrature. Observing near quadrature ensured a sufficiently large Doppler shift between Earth and Jupiter to separate the terrestrial and Jovian CH_4 lines (see Table 1 for the Doppler velocity during each run). In order to measure short-term variability, we aimed to repeat our observations at both the beginning and end of a given observing run, however weather conditions meant that this was not always possible. In total, these observations provide comparisons over 1-week, 1-month and 4-month intervals.

2.2. Data reduction

The individual scans of Jupiter were each reduced using the data reduction pipeline described in Lacy et al. (2002). This software performs flat fielding and sky subtraction, and then removes instrumental geometric optical distortions. Wavelength calibration was achieved by using telluric absorption lines and radiometric calibration was achieved by using the measured radiance of a room temperature blackbody that is automatically placed in

front of instrument aperture prior to each set of observations. The noise of each spectral data point was calculated following the method described for TEXES observations in Greathouse et al. (2011).

The pipeline-reduced data products were then geometrically calibrated, cylindrically projected and co-added. The scan parameters were used to calculate the shape of the planet’s limb, which was then fitted to each observation by eye. This allows each pixel to be assigned a latitude and longitude. The Doppler shift of the spectrum was calculated for each pixel, comprising both a component due to the Earth-Jupiter velocity and a position-dependent component due to Jupiter’s rotation (zonal wind speeds are negligible in comparison); this Doppler shift was removed for each pixel, shifting the Jovian spectrum into the rest frame. The observations were then binned according to airmass and then projected onto a latitude-longitude grid; this allows multiple scans to be co-added to produce a single data cube per airmass bin.

3. Spectral modeling

The TEXES spectra were modeled using a radiative transfer and retrieval code that has previously been used to model the stratospheres of Saturn (Greathouse et al., 2005) and Neptune (Greathouse et al., 2011). The code is made up of a line-by-line radiative transfer code that calculates the theoretical spectrum for a given atmospheric profile and an optimal estimation retrieval code that uses a Levenberg-Marquardt approach to iteratively adjust the atmospheric parameters and achieve an optimal fit between the theoretical spectrum and the observed spectrum (Rodgers, 2000). The code is described in greater depth in Greathouse et al. (2011).

For this study, Jupiter’s atmosphere was divided into 95 levels between 4 bar and 1×10^{-7} bar, equally spaced in $\log(p)$. The vertical distribution of CH_4 was obtained from the photochemical model of Moses et al. (2005), which takes into account both eddy mixing and molecular diffusion. The line data for $^{12}\text{CH}_4$, $^{13}\text{CH}_4$ and $^{12}\text{CH}_3\text{D}$ were obtained from the HITRAN molecular database (Rothman et al., 2005), and the temperature dependence of the line widths in an H_2 atmosphere was obtained from Margolis (1993). Collision induced absorption data for H_2 – H_2 , H_2 – He and H_2 – CH_4 were included from Orton et al. (2007), Borysow et al. (1988) and Borysow and Frommhold (1986) respectively. We assume local thermodynamic equilibrium (LTE) at all pressure levels; our observations are primarily sensitive to pressures in the 0.1–30 mbar range, and the transition between LTE and non-LTE does not occur until $\sim 1 \mu\text{bar}$ (Drossart et al., 1999).

The a priori vertical temperature profile is based on the model described in Moses et al. (2005). This profile was allowed to vary in the retrievals, in order to fit the TEXES spectra. The temperature is retrieved at each of the 95 pressure levels and a correlation length of 1 scale height is used to prevent unphysically sharp deviations between

Date	Longitudinal coverage at the equator (%)	Angular diameter (arcsec)	Earth-Jupiter velocity (km/s)	Sub-solar planetocentric latitude (°)	Heliocentric distance (AU)
Jan 2012	72	41	28	3.07	4.98
Sep 2012	100	44	-24	2.92	5.04
Feb 2013	100	42	27	2.68	5.08
Feb 2014	100	43	23	1.44	5.21
Dec 2014	78	41	-25	0.23	5.31
Mar 2015	100	41	25	-0.26	5.35
Nov 2015	100	34	-26	-1.17	5.41
Jan 2016	100	41	-24	-1.39	5.42
Apr 2016	100	41	24	-1.76	5.44
Jan 2017	100	37	-28	-2.51	5.46
May 2017	100	41	23	-2.79	5.45
Jul 2017	61	36	27	-2.86	5.45
Feb 2018	100	37	-29	-3.07	5.43
Jul 2018	100	40	25	-3.07	5.40
Sep 2018	100	34	22	-3.02	5.38
Feb 2019	100	35	-26	-2.84	5.34
Apr 2019	100	42	-23	-2.72	5.32
Aug 2019	100	40	25	-2.44	5.28

Table 1: Summary of IRTF observing runs contributing to this study: the month and year, the longitudinal coverage obtained over the course of the observing run, Jupiter’s angular diameter as observed from the Earth, the Doppler velocity, the sub-solar Jovian latitude and the distance of Jupiter from the sun.

adjacent levels. Figure 1 shows an example of a fitted spectrum and a retrieved temperature profile for data obtained on 17–18 November 2015. Figure 1(a) shows the TEXES spectrum in black, along with the best-fit model spectrum in red. The gap in the data at 1247.7 cm^{-1} is due to the presence of a strong telluric line. Figure 1(b) shows the corresponding retrieved vertical temperature profile along with the a priori temperature profile. The error bars shown in Figure 1(b) represent the formal uncertainty in the retrieval. They are a minimum at ~ 13 mbar, the pressure level of maximum sensitivity. As the pressure increases, the formal error bars also increase, but do not fully capture the dependence on any assumed model parameters in the deeper atmosphere. We consider the retrievals to be robust in the 0.1–30 mbar region. Within this region, the formal error bars are ~ 1.5 K; in the subsequent sections, we adopt a more conservative error of 2 K to include systematic effects (Cosentino et al., 2017).

The radiative transfer and retrieval code was applied to all of the observations described in Section 2 in order to produce both two-dimensional and three-dimensional temperature maps for each observing date. As the QGO is an oscillation pattern in the global-scale wind field, we are primarily interested in the two-dimensional, zonally-averaged temperature maps. As described in Section 2, the TEXES spectral data were binned according to latitude, longitude and Jovian airmass. Data obtained from several nights on each observing run were then co-added to provide as complete longitudinal coverage as possible. The data were then averaged across all longitudes, in order to produce a single

spectrum for each latitude (2° bins) and airmass (four bins, covering airmasses of 1–5). For each latitude, the retrieval code was used to simultaneously fit the different airmass spectra, in order to produce a final vertical temperature profile for that latitude. Combining the vertical temperature profiles for each latitude produces a two-dimensional temperature map. These zonally-averaged maps are the focus of Sections 4.1 and 4.2.

The observational data were also used to produce zonally-resolved three-dimensional maps. These were generated by retrieving the vertical temperature profile at each longitude and latitude point, instead of averaging across the longitudinal dimension. This allows us to search for spatially-localized thermal anomalies, as shown in Section 4.3.

An example of a retrieved zonally-averaged temperature map from 17–18 November 2015 is shown in Figure 2(a). The dashed lines in the figure show latitudes of 14°S , 0° and 14°N , the locations of the main equatorial QGO signature and the anti-phase components. Figure 2(a) shows a clear vertical oscillation in temperature at the equator, with a strong local minimum (relative to the off-equatorial $\pm 14^\circ$ temperatures) at approximately 8 mbar and strong local maxima at approximately 2 mbar and 20 mbar. This is highlighted by Figure 2(b), which shows the temperatures as a function of latitude for 2 mbar and 8 mbar.

This vertical oscillation is a signature of the QGO; as time passes the local maxima and minima at the equator move to deeper pressure levels. To study this, comparable temperature maps were made for each observing run

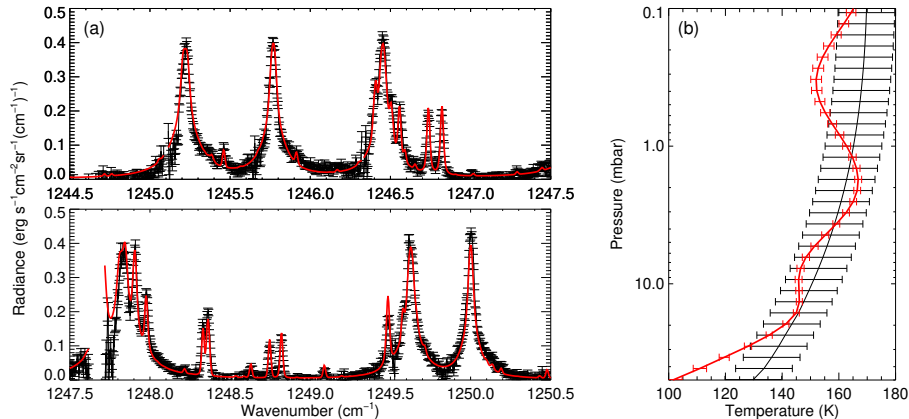


Figure 1: (a) An example of a zonally-averaged equatorial TEXES spectrum from 17–18 November 2015 (black) along with the best-fit model spectrum (red). The spectrum is split into two frames to make the features more clear. (b) Corresponding vertical temperature profile (red), along with the a priori temperature profile (black).

conducted in 2012–2019 (Table 1). The evolution of the stratospheric temperatures with time is described and discussed in Section 4. Section 4.1 discusses the evolution of Jupiter’s QJO over the 2012–2017, while Section 4.2 discusses an apparent disruption in the QJO pattern in 2017.

We note that Figure 2 also shows other interesting phenomena, such as a vertical temperature oscillation in the mid-latitudes (± 20 – 30°). However, no oscillation is observed at these latitudes and there is therefore no clear link with the QJO. Analysis of the retrieved mid-latitude temperatures is therefore outside the scope of this paper.

4. Results and discussion

4.1. Behavior of the QJO in 2012–2017

Figure 3 shows the time series of Jupiter’s equatorial temperature oscillation during the entire 2012–2019 observation period. All observations from a given observing run are combined into a single zonally-averaged temperature retrieval. The retrieved temperatures are the average from the 2°S – 2°N latitude range and the temperature offset at each pressure level is defined as the zonally-averaged temperature relative to the average of the maximum and minimum temperature in 2012–2016 (corresponding to a complete, unperturbed oscillation).

Figure 3 is analogous to the time-height diagrams of the Earth’s QJO, as seen in e.g. Naujokat (1986). As with the QJO, the QJO consists of downward propagating warm and cool regions, causing the temperature at a given pressure level to oscillate with time. With the Earth’s QJO, the time taken for the pattern to repeat is approximately two years, and for Jupiter’s QJO, the period is approximately four years. On Earth, wind speeds can be measured directly and so time-height diagrams are typically presented in terms of winds. However, the wind shear and temperatures are coupled via the thermal wind equation (which for Earth remains valid deep into the tropics,

Allen and Sherwood, 2007); positive (eastward/westerly) vertical wind shear in the QJO is correlated with warm equatorial anomalies (Pascoe et al., 2005).

Figure 4 presents the QJO data for three different pressure levels: 3.0 mbar, 6.4 mbar and 13.5 mbar. The red data points correspond to the same equatorial data that are shown in Figure 3. The dashed lines in Figure 3 highlight the three pressure levels used in Figure 4. Alongside the equatorial temperature offsets, we also present the temperature offsets for 14°N (black) and 14°S (blue).

The long-term $7.8\text{-}\mu\text{m}$ images that were first used to identify the QJO (Orton et al., 1991; Leovy et al., 1991) are sensitive to the 10–20 mbar pressure range; Figure 4(c) therefore provides the best comparison with those results. This pressure levels also corresponds to the region of maximum sensitivity for the TEXES data. Figure 4(c) shows a clear sinusoidal pattern for the first five years of the data collection (2012–2017). Fitting a sine curve to the pre-2017 red equatorial data results in a period of 4.0 ± 0.2 years; the fitted curve is shown by the red dashed line. The amplitude of this fitted oscillation at 13.5 mbar is 7 ± 1 K. The 14°N and 14°S temperatures also show a roughly sinusoidal pattern at 13.5 mbar for the first five years, which is in anti-phase to the equatorial temperatures and has a comparable magnitude. This agrees with previous IRTF observations which showed that the $7.8\text{-}\mu\text{m}$ brightness is anti-correlated between the equator and $\pm 13^\circ$ (Friedson, 1999).

As previously discussed in Cosentino et al. (2017), the vertically-resolved TEXES observations show for the first time that Jupiter’s QJO extends to lower pressures. This can be clearly seen in Figure 3, which shows the diagonal, downward propagating pattern extend between ~ 1 mbar and ~ 20 mbar. At pressures less than 1 mbar, no clear oscillation is observed, although it should be noted that our sensitivity begins to decrease at these pressures.

Figures 4(a) and (b) show how the QJO oscillations appear at pressures of 3.0 mbar and 6.4 mbar. The 2012–2017

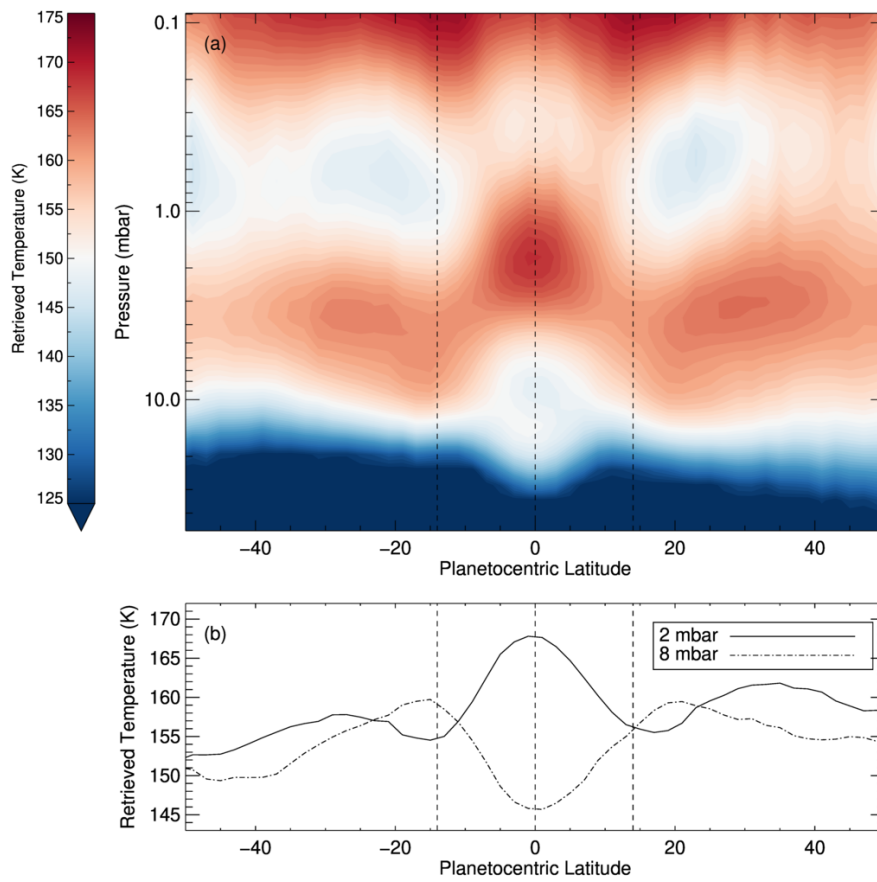


Figure 2: (a) Example of a zonally-averaged retrieved temperature map from 17–18 November 2015. The vertical dashed lines show latitudes of 14°S, 0° and 14°N, the three latitudes that are shown in Figure 4. (b) Slices through (a) at two different pressures levels representing a local maximum at the equator (2 mbar) and a local minimum at the equator (8 mbar).

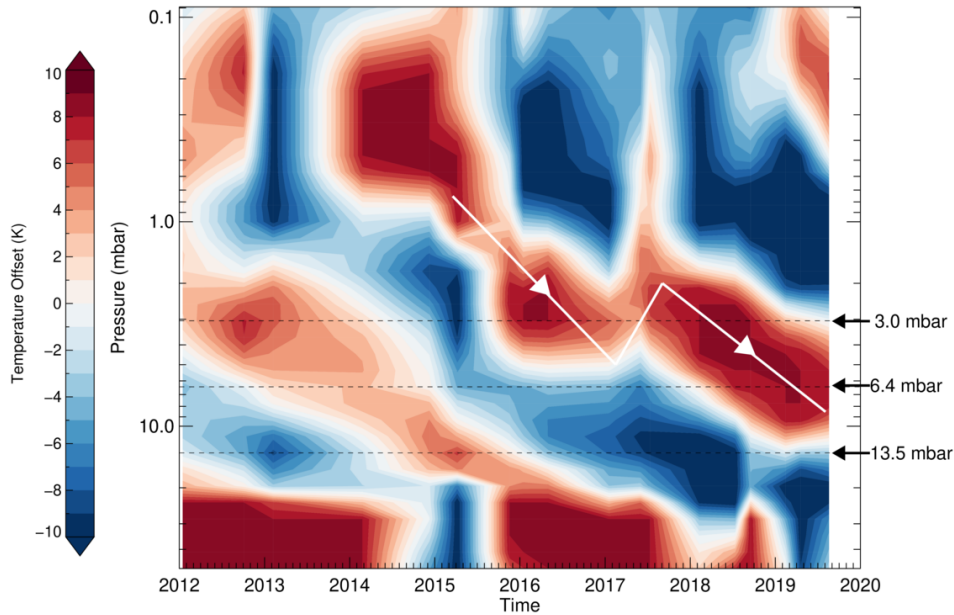


Figure 3: Time series of Jupiter’s QJO from 2012–2019 as a function of pressure and time. The retrieved temperatures are from Jupiter’s equator (2°S – 2°N) and the temperature offset for each pressure level is defined as the zonally-averaged temperature relative to the average of the maximum and minimum temperature during the first four years of data (corresponding to a complete, unperturbed oscillation). The dashed black lines highlight the 3.0-mbar, 6.4-mbar and 13.5-mbar pressure levels that are shown in Figure 4. The white line shows an apparent disruption in the descending warm branch.

data in these figures show that the equatorial temperatures at these lower pressures still exhibit an approximately sinusoidal pattern. The dashed red lines in Figures 4(a) and (b) show the best-fit sine curve to the 2012–2017 equatorial data, assuming the same 4.0-year period derived from Figure 4(c). At 6.4 mbar, the oscillation is still a smooth sine wave; at 3.0 mbar, it appears to be more ‘sawtooth’. At these higher altitudes, any oscillation in the off-equatorial temperatures is significantly weaker than at 13.5 mbar.

4.2. Disruption of the QJO in 2017

The temperature offsets in 2012–2017 appear to show a ‘typical’ QJO pattern, consisting of a smoothly varying sinusoidal oscillation with a period of ~ 4 years. However, Figures 3 and 4 show that there is a phase-shift disruption to this pattern in mid-2017.

The equatorial data, shown in red in Figure 4(c), show that the temperatures continue to decrease in late 2017 / early 2018, rather than following the 4-year-period sinusoidal pattern shown by the dashed red line. This leads to the minimum in the equatorial 13.5-mbar temperature occurring ~ 1 year later than expected. Similar shifts can be observed in Figures 4(a) and (b). In Figure 4(b), the equatorial data lags ~ 1 year behind the nominal sinusoid from 2017 onwards. In Figure 4(a), the change is even more stark. In 2017–2018, we would expect the equatorial 3-mbar temperatures to be decreasing, reaching a minimum in late 2018. Instead, the temperatures start to decrease as expected, but then suddenly tick upwards in mid-2017, reaching a local maximum in early 2018, just two years

after the previous local maximum. When the equatorial temperatures start to decrease again, they are ~ 1 year behind schedule.

Figure 4 also shows how the off-equatorial temperatures vary from 2017 onward. Figure 4(c) shows that the $\pm 14^{\circ}$ temperatures broadly continue in anti-phase with the equatorial temperatures. In particular, it can be seen that the 14°N temperature peaks in early 2018, at the same time as the equatorial temperatures reach their delayed minimum. The off-equatorial results shown in Figures 4(b) and (c) also show a change in 2017. Before 2017, the $\pm 14^{\circ}$ temperature offsets are relatively flat. From mid-2017 onward, the 14°S temperatures continue to be mostly flat, but the 14°N temperatures show a stronger inverse correlation with the equatorial temperatures.

Further insight into how the equatorial temperatures evolved over this time period can be obtained from Figure 3. The solid white line shows the motion of the descending warm branch of the QJO. In 2017, this warm branch undergoes an abrupt upward displacement. This has the effect of ‘delaying’ the QJO by ~ 1 year at the 3.0-mbar, 6.4-mbar and 13.5-mbar pressure levels, as shown in Figure 4. The upwards displacement of the descending warm branch coincides with an abrupt, short-lived warming at high altitudes (0.2–2 mbar).

The QJO disruption observed in Figures 3 and 4 bears some similarities to the disruption of the Earth’s QBO that was observed in 2015–2016 (Osprey et al., 2016; Newman et al., 2016). The QBO has been observed continuously using tropical radiosonde wind observations since 1953 and

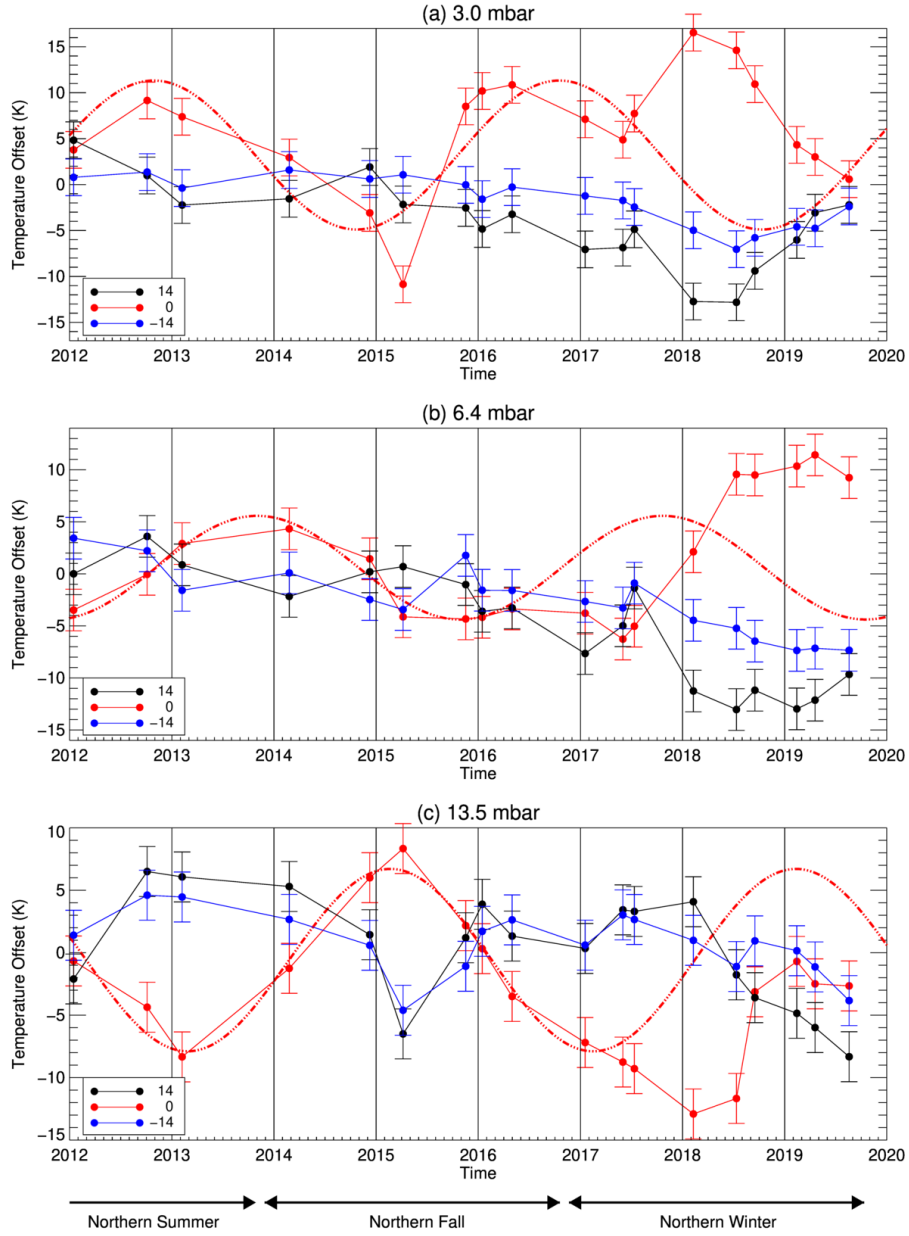


Figure 4: Time series of Jupiter’s QQO from 2012–2019, showing the temperature offsets at (a) 3.0 mbar, (b) 6.4 mbar and (c) 13.5 mbar. Each plot shows retrieved temperatures from three different latitudes: 14°N (black), 0° (red) and 14°S (blue). The temperature offset for each pressure level is defined as the zonally-averaged temperature relative to the average of the maximum and minimum temperature during the first four years of data (corresponding to a complete, unperturbed oscillation). The dashed red lines show a sinusoidal curve with a period of 4.0 years (the best-fit period for the 2012–2017 13.5-mbar data). Jupiter’s seasons are labelled at the bottom.

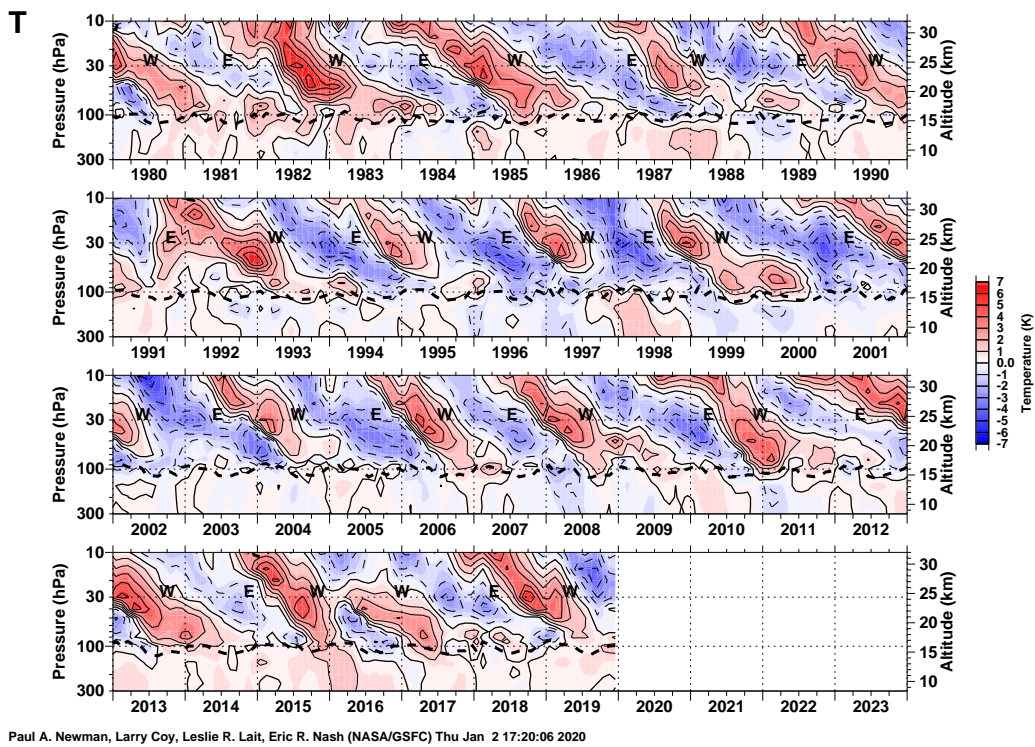


Figure 5: Earth's equatorial QBO from 1980–2020; figure from NASA/GSFC Data Services (https://acd-ext.gsfc.nasa.gov/Data_services/met/qbo/qbo.html). Radiosonde temperature data were obtained from the Meteorological Service Singapore Upper Air Observatory and the data have been detrended and the annual cycle has been removed. The 2015–2016 QBO disruption can be clearly seen (Newman et al., 2016).

is ordinarily one of the most repeatable phenomena in the Earth’s atmosphere, with an oscillation period that has varied between 22 and 34 months (Baldwin et al., 2001). In 2015–2016, a disruption was observed in the typical QBO pattern for the first time in over sixty years of observations. Osprey et al. (2016) and Newman et al. (2016) show the QBO disruption in terms of the zonal winds; Figure 5 shows the disruption in terms of the stratospheric temperature anomalies, allowing it to be directly compared with Figure 3. Newman et al. (2016) describe the disruption as an apparent upward displacement of an anomalous westerly wind and the development of easterlies at 40 mbar; this has the effect of altering the short-term behavior of the oscillation, producing an unusually long-lasting 23-month eastward phase at 20 mbar, compared to the average 14-month duration (Kumar et al., 2018). In the temperature data shown in Figure 5, this manifests as an upward displacement in the warm branch and the development of a new cold branch at 40 mbar.

This is morphologically similar to Figure 3, which shows an upward displacement of the QJO’s descending warm branch in 2017. As with the 2015–2016 QBO disruption, this has the effect of altering the short-term behavior of the QJO, producing an unusually long cold phase at 13.5 mbar. However, we should note that the QBO disruption in 2015–2016 was a highly unusual event; the earth’s wind patterns and temperatures have been consistently tracked for over 60 years, providing a vertically-resolved long-term dataset, and Figure 5 shows that this was a unique event within that time period. In contrast, it is unclear whether the QJO disruption shown in Figure 3 is an uncommon event, as vertically-resolved measurements of the QJO have only been made since 2012. 7.8- μm imaging data have been made since 1980 (Orton et al., 1991; Leovy et al., 1991), but these observations do not provide vertical resolution and are therefore not able to fully capture the effect of a vertical displacement of the QJO; it is possible that some of the variability in the oscillation period observed in the imaging data (Simon-Miller et al., 2006) is due to a similar type of disruption.

4.3. Potential causes of the 2017 disruption

Based on Figures 3 and 4, we conclude that there was a disruption to the QJO pattern in 2017; this disruption consisted of an upward displacement of the descending warm branch, leading to a phase shift in the oscillation. Numerical modeling of the observed disruption is beyond the scope of this paper and will be a subject for future study. Instead, we discuss here the causes of similar disruptions on other planets and present observations of a high-altitude thermal anomaly that may be linked to the observed disruption.

Barton and McCormack (2017) found that the Earth’s QBO disruption in 2015–2016 was caused by the propagation of Rossby waves from the extratropical Northern Hemisphere. The combination of the timing of the QBO relative to the annual cycle and an extreme El Niño event

meant that the subtropical easterly jet in the winter lower stratosphere was unusually weak; this allowed westward-moving Rossby waves to propagate southwards into the equatorial region, and deposit a large flux of westward momentum at 40 mbar.

Like the Earth and Jupiter, Saturn also has an oscillation in the equatorial stratosphere. This oscillation is known as Saturn’s Semi-Annual Oscillation (SSAO) and it has a period of 14.7 ± 0.9 years (Orton et al., 2008; Fouchet et al., 2008). Fletcher et al. (2017a) found that in 2011–2014, the SSAO was disrupted by an intense storm in the northern mid-latitudes. The storm consisted of powerful convective plumes in the troposphere, and led to the formation of a large, hot, westward-moving vortex in the stratosphere at 40°N (Fletcher et al., 2012). This vortex (known as the ‘beacon’) persisted for over three years, significantly longer than the tropospheric storm. At its peak, the beacon had a temperature that was 80 K higher than the surrounding quiescent regions at 2 mbar. During the same time period, Fletcher et al. (2017a) showed that the SSAO signature was essentially absent, before resuming in 2014. As with the Earth’s QBO disruption, Fletcher et al. (2017a) attribute the SSAO disruption to an injection of westward momentum in the equatorial regions by extratropical waves; in this case, the waves were thought to be driven by the hot beacon and/or the underlying storm.

As both the QBO disruption and the SSAO disruption were caused by the propagation of extratropical waves, we used the TEXES zonally-resolved temperatures maps to search for any unusual behavior that could be associated with the 2017 QJO disruption. We found a high-altitude, mid-latitude thermal anomaly in the May/June 2017 data, the same observing run in which the disruption was first observed; an inspection of the spatially-resolved temperature maps from the other observing runs showed that this was the largest thermal anomaly observed over the eight year time period.

The May/June 2017 thermal anomaly is shown in Figures 6 and 7. Figure 6 shows three different slices through the three-dimensional temperature map obtained using data from May 28–29. The temperature offset is defined as the temperature relative to the mean zonal temperature at a given pressure and latitude level. The average retrieved error on the temperature offsets is ~ 2 K. Figure 6(a) shows the thermal anomaly as a function of pressure and longitude, at a latitude of 28°N ; 6(b) shows the thermal anomaly as a function of latitude and longitude, at a pressure of 1.2 mbar; and 6(c) shows the thermal anomaly as a function of latitude and pressure, at a longitude of 178°W . In each case, the dashed black lines highlight the latitude, longitude and pressure of interest; the three images intersect at the intersection of the dashed black lines. Figure 7 shows a comparable set of images for data obtained on June 5.

Both Figures 6 and 7 show a warm high-altitude double-peaked thermal anomaly centered at a latitude of 28°N and a pressure of 1.2 mbar. This is located in Jupiter’s North

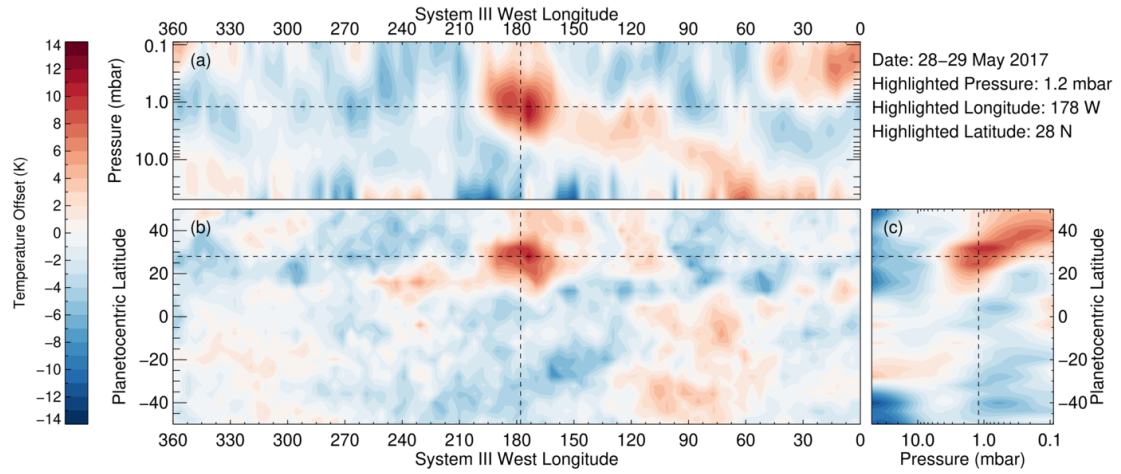


Figure 6: A warm thermal anomaly, as seen on May 28–29 2017. The three frames show three orthogonal slices through a three-dimensional retrieved temperature map; these slices are centered on a warm thermal anomaly. The temperature offset is defined as the temperature relative to the mean zonal temperature at a given pressure and latitude level.

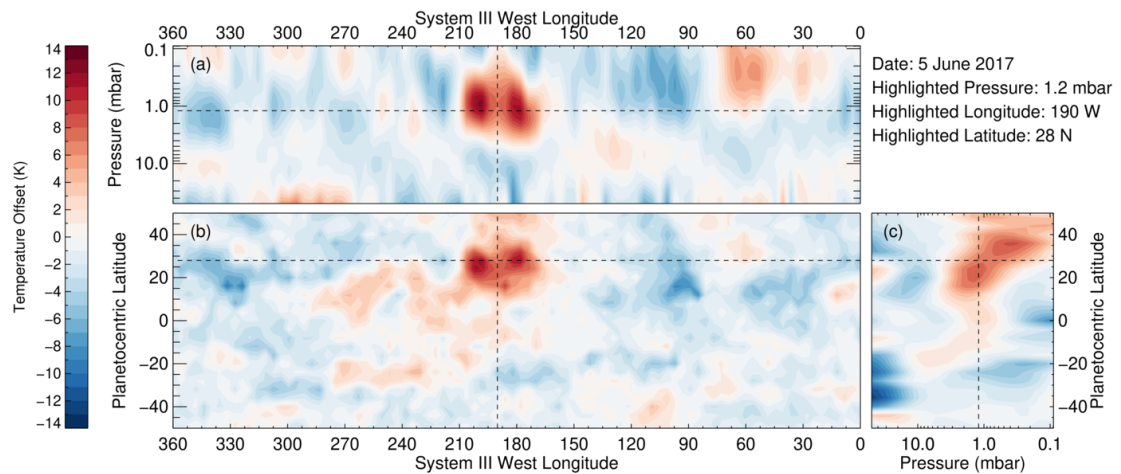


Figure 7: The same thermal anomaly shown in Figure 6, as seen on June 5 2017.

Temperate Belt, northwards of the planet’s strong prograde jet at 23°N (Porco et al., 2003). By fitting a Gaussian curve to the retrieved temperatures as a function of longitude, we find that the thermal anomaly moves westward with a velocity of 1.5 ± 0.3 degrees/day; at a latitude of 28°N, this is equivalent to 19 ± 4 ms⁻¹. No anomaly was present at the same latitude and pressure region during the January 2017 or February 2018 observing runs. It was also not observed in July 2017, although full longitudinal coverage was not obtained on this occasion and the relevant longitudes were not observed (assuming a constant velocity of 1.5 degrees/day).

The correlation between the timing of this thermal anomaly and the disruption of the QQQ is suggestive of a link between these two events. In addition, the thermal anomaly has some features in common with the stratospheric ‘beacon’ on Saturn that disrupted the SSAO; this thermal anomaly is also a westward-moving hotspot in the stratospheric mid-latitudes. However, the scales of the two hotspots are very different. Saturn’s beacon was 80 K warmer than its surroundings and persisted for over three years, while the thermal anomaly we observe here was 13 K warmer than its surroundings and persisted for less than seven months. It is unclear whether a thermal anomaly on this smaller scale would have the capacity to influence the equatorial temperatures.

Jupiter’s troposphere undergoes large-scale upheavals relatively frequently. These events have the ability to dramatically change the appearance of the planet by altering the cloud structure (Sánchez-Lavega et al., 2008; Fletcher et al., 2017b) and would be plausible candidates for driving a disruption in the QQQ and/or causing localized thermal anomalies in the stratosphere; rather than causing the disruption directly, one possibility is that both the thermal anomaly and the QQQ disruption are the result of a localized storm deep in Jupiter’s troposphere. However, there were no notable planetary scale disturbances during the 2017–2018 timeframe that we can easily tie to the QQQ disturbance, despite an extensive search of images from different sources.

Sánchez-Lavega et al. (2017) report on a large disturbance in Jupiter’s North Temperate Belt in October 2016, consisting of a set of four powerful plumes located at 23°N, that moved eastward with time. However, this activity had ceased by late November 2016, seven months before the QQQ disturbance and the mid-latitude thermal anomaly were observed. Wong et al. (2020) present an archive of high spatial resolution images of Jupiter in the 2016–2020 time period; their observations provide good temporal coverage in the spring–summer 2017 timeframe and include full longitudinal coverage in the visible from Hubble’s Wide Field Camera 3 in April 2017, but they note no large convective storm in the northern low or mid latitudes beside the one observed in October 2016. Antuñaño et al. (2018) describe a pattern of semi-regular disturbances in Jupiter’s equatorial zone, occurring with a periodicity of 6–8 or 13–14 years. These disturbances consist of a dra-

matic clearing in Jupiter’s equatorial cloud layer, resulting in a sharp increase in the 5- μ m brightness. The most recent disturbance described in Antuñaño et al. (2018) occurred in 2006–2007, and they predicted a new equatorial zone disturbance in 2019–2021. Changes in the 5- μ m brightness began to be observed in late 2018 (Orton et al., 2019), over a year after the QQQ disruption. Finally, we consulted the archives of the British Astronomical Association (BAA¹), who keep a detailed record of observations of Jupiter made by amateur astronomers. BAA reports carefully document the outbreak in the North Temperate Belt in October 2016, but there was no similar outbreak observed in spring/summer 2017, despite a large dataset of observations (Rogers, 2017).

While Jupiter’s troposphere exhibits constant activity, the 2017 QQQ disruption does not appear to coincide with any large global-scale tropospheric upheaval events that could be seen in visible or infrared observations. It is possible that a storm could have been present deeper in Jupiter’s atmosphere, below the visible cloud deck, but it is difficult to see how such a storm could affect stratospheric temperatures without causing a visible plume. Further monitoring of Jupiter’s stratospheric and tropospheric temperatures will be required to make further progress in understanding the causality of such events in Jupiter’s atmosphere.

5. Conclusions

In this paper, we used high-resolution mid-infrared data from TEXES/IRTF to track the evolution of Jupiter’s quasi-quadrennial oscillation (QQO) over the course of approximately two full cycles (2012–2019). We used a radiative transfer model to retrieve the zonally-averaged and zonally-resolved atmospheric temperatures in the 0.01–30 mbar pressure range. Using the temperature maps obtained from these retrievals, we come to the following conclusions:

1. Between 2012 and 2017, the 13.5-mbar equatorial temperatures had a smoothly sinusoidal pattern with a period of 4.0 ± 0.2 years and an amplitude of 7 ± 1 K at 13.5 mbar (our region of maximum sensitivity). During this same time period, the 13.5-mbar temperatures at $\pm 14^\circ$ were in anti-phase with the equatorial temperatures. This is consistent with previous studies of the QQQ (Orton et al., 1991; Friedson, 1999).
2. Between 2012 and 2017, the 6.4-mbar and 3.0-mbar equatorial temperatures also displayed an approximately sinusoidal pattern, with a similar period. This extension of the QQQ up to these lower pressure levels was a new result presented in Cosentino et al. (2017) using the 2012–2016 TEXES data.

¹britastro.org

3. In 2017, there was a disruption to the QQO pattern. This disruption is evident at 3-20 mbar, and appears to manifest as an abrupt upward displacement of the descending warm branch. This disruption has similarities to the disruption of the Earth's QBO in 2015–2016.
4. In May/June 2017, we observed a localized warm thermal anomaly located at a latitude of 28°N and a pressure of 1.2 mbar. By comparing observations made ~1 week apart, we found that this thermal anomaly was moving westward with a velocity of $19 \pm 4 \text{ ms}^{-1}$

Based on the timing of the warm thermal anomaly, there is a possibility that it may be related to the QQO disruption that we observe. We note that a hot thermal anomaly in Saturn's mid-latitude stratosphere was linked to a disruption in the SSAO. However, the warm anomaly that we observe in Jupiter's stratosphere is significantly cooler (~13 K) and it is unclear whether it would have a significant impact on the equatorial regions. One possibility is that both the thermal anomaly and the QQO disruption are the result of storms deep in Jupiter's troposphere, although no unusual activity was observed during this time period. Future modelling work is required to better understand the factors that drive changes to Jupiter's QQO.

Acknowledgments

This research was primarily funded by NASA Planetary Astronomy (PAST) grant NNX14AG34G. GSO was supported by funds from NASA distributed to the Jet Propulsion Laboratory, California Institute of Technology. This work was based on data obtained with the NASA Infrared Telescope Facility, which is operated by the University of Hawaii under a contract with the National Aeronautics and Space Administration. The authors would like to acknowledge the contributions of many observing collaborators and NASA/IRTF staff. The authors would also like to thank the two anonymous reviewers whose comments helped improve and clarify this manuscript.

References

References

Allen, R.J., Sherwood, S.C., 2007. Utility of radiosonde wind data in representing climatological variations of tropospheric temperature and baroclinicity in the western tropical Pacific. *Journal of Climate* 20, 5229–5243.

Antuñano, A., Fletcher, L.N., Orton, G.S., Melin, H., Rogers, J.H., Harrington, J., Donnelly, P.T., Rowe-Gurney, N., Blake, J.S., 2018. Infrared characterization of Jupiter's equatorial disturbance cycle. *Geophysical Research Letters* 45, 10987–10995.

Baldwin, M., Gray, L., Dunkerton, T., Hamilton, K., Haynes, P., Randel, W., Holton, J., Alexander, M., Hirota, I., Horinouchi, T., et al., 2001. The quasi-biennial oscillation. *Reviews of Geophysics* 39, 179–229.

Barton, C., McCormack, J., 2017. Origin of the 2016 QBO disruption and its relationship to extreme El Niño events. *Geophysical Research Letters* 44, 11150–11157.

Borysow, A., Frommhold, L., 1986. Theoretical collision-induced rototranslational absorption spectra for the outer planets: H₂-CH₄ pairs. *The Astrophysical Journal* 304, 849–865.

Borysow, J., Frommhold, L., Birnbaum, G., 1988. Collision-induced rototranslational absorption spectra of H₂-He pairs at temperatures from 40 to 3000 K. *The Astrophysical Journal* 326, 509–515.

Brown, L.R., Benner, D.C., Champion, J.P., Devi, V.M., Fejard, L., Gamache, R., Gabard, T., Hilico, J., Lavorel, B., Loete, M., et al., 2003. Methane line parameters in HITRAN. *Journal of Quantitative Spectroscopy and Radiative Transfer* 82, 219–238.

Cosentino, R.G., Morales-Juberías, R., Greathouse, T., Orton, G., Johnson, P., Fletcher, L.N., Simon, A., 2017. New observations and modeling of Jupiter's quasi-quadrennial oscillation. *Journal of Geophysical Research: Planets* 122, 2719–2744.

Drossart, P., Fouchet, T., Crovisier, J., Lellouch, E., Encrenaz, T., Feuchtgruber, H., Champion, J., 1999. Fluorescence in the 3 micron bands of methane on Jupiter and Saturn from ISO/SWS observations, in: *The Universe as seen by ISO*, p. 169.

Dunkerton, T.J., 1997. The role of gravity waves in the quasi-biennial oscillation. *Journal of Geophysical Research: Atmospheres* 102, 26053–26076.

Flasar, F.M., Kunde, V., Achterberg, R., Conrath, B., Simon-Miller, A., Nixon, C., Gierasch, P., Romani, P., Bézard, B., Irwin, P., et al., 2004. An intense stratospheric jet on Jupiter. *Nature* 427, 132–135.

Fletcher, L.N., Guerlet, S., Orton, G.S., Cosentino, R.G., Fouchet, T., Irwin, P.G., Li, L., Flasar, F.M., Gorius, N., Morales-Juberías, R., 2017a. Disruption of Saturn's quasi-periodic equatorial oscillation by the Great Northern Storm. *Nature Astronomy* 1, 765.

Fletcher, L.N., Hesman, B., Achterberg, R., Irwin, P., Bjoraker, G., Gorius, N., Hurley, J., Sinclair, J., Orton, G., Legarreta, J., et al., 2012. The origin and evolution of Saturn's 2011–2012 stratospheric vortex. *Icarus* 221, 560–586.

Fletcher, L.N., Orton, G., Rogers, J., Giles, R., Payne, A., Irwin, P., Vedovato, M., 2017b. Moist convection and the 2010–2011 revival of Jupiter's South Equatorial Belt. *Icarus* 286, 94–117.

Fouchet, T., Guerlet, S., Strobel, D., Simon-Miller, A., Bézard, B., Flasar, F., 2008. An equatorial oscillation in Saturn's middle atmosphere. *Nature* 453, 200.

Friedson, A.J., 1999. New observations and modelling of a QBO-like oscillation in Jupiter's stratosphere. *Icarus* 137, 34–55.

Greathouse, T.K., Lacy, J.H., Bézard, B., Moses, J.I., Griffith, C.A., Richter, M.J., 2005. Meridional variations of temperature, C₂H₂ and C₂H₆ abundances in Saturn's stratosphere at southern summer solstice. *Icarus* 177, 18–31.

Greathouse, T.K., Richter, M., Lacy, J., Moses, J., Orton, G., Encrenaz, T., Hammel, H., Jaffe, D., 2011. A spatially resolved high spectral resolution study of Neptune's stratosphere. *Icarus* 214, 606–621.

Kumar, K.K., Mathew, S.S., Subrahmanyam, K., 2018. Anomalous tropical planetary wave activity during 2015/2016 quasi biennial oscillation disruption. *Journal of Atmospheric and Solar-Terrestrial Physics* 167, 184–189.

Lacy, J., Richter, M., Greathouse, T., Jaffe, D., Zhu, Q., 2002. TEXES: A sensitive high-resolution grating spectrograph for the mid-infrared. *Publications of the Astronomical Society of the Pacific* 114, 153–168.

Leovy, C.B., Friedson, A.J., Orton, G.S., 1991. The quasi-quadrennial oscillation of Jupiter's equatorial stratosphere. *Nature* 354, 380.

Li, X., Read, P., 2000. A mechanistic model of the quasi-quadrennial oscillation in Jupiter's stratosphere. *Planetary and Space Science* 48, 637–669.

Margolis, J.S., 1993. Measurement of hydrogen-broadened methane lines in the ν_4 band at 296 and 200 K. *Journal of Quantitative Spectroscopy and Radiative Transfer* 50, 431–441.

Moses, J., Fouchet, T., Bézard, B., Gladstone, G., Lellouch, E., Feuchtgruber, H., 2005. Photochemistry and diffusion in Jupiter's stratosphere: constraints from ISO observations and comparisons with other giant planets. *Journal of Geophysical Research: Planets* 110.

Naujokat, B., 1986. An update of the observed quasi-biennial oscillation.

lation of the stratospheric winds over the tropics. *Journal of the Atmospheric Sciences* 43, 1873–1877.

Newman, P., Coy, L., Pawson, S., Lait, L., 2016. The anomalous change in the QBO in 2015–2016. *Geophysical Research Letters* 43, 8791–8797.

Orton, G., Antuñaño, A., Fletcher, L., Sinclair, J., Momary, T., Chowdhury, N., Melin, H., Stallard, T., Rathbun, J., Bjoraker, G., et al., 2019. Juno and Juno-supporting observations of Jupiter’s 2018-2019 equatorial zone disturbance, in: EPSC Abstracts.

Orton, G.S., Friedson, A.J., Baines, K.H., Martin, T.Z., West, R.A., Caldwell, J., Hammel, H.B., Bergstralh, J.T., Malcom, M.E., Golisch, W.F., et al., 1991. Thermal maps of Jupiter: spatial organization and time dependence of stratospheric temperatures, 1980 to 1990. *Science* 252, 537–542.

Orton, G.S., Gustafsson, M., Burgdorf, M., Meadows, V., 2007. Revised ab initio models for H₂-H₂ collision-induced absorption at low temperatures. *Icarus* 189, 544–549.

Orton, G.S., Yanamandra-Fisher, P.A., Fisher, B.M., Friedson, A.J., Parrish, P.D., Nelson, J.F., Bauermeister, A.S., Fletcher, L., Gezari, D.Y., Varosi, F., et al., 2008. Semi-annual oscillations in Saturn’s low-latitude stratospheric temperatures. *Nature* 453, 196.

Osprey, S.M., Butchart, N., Knight, J.R., Scaife, A.A., Hamilton, K., Anstey, J.A., Schenzinger, V., Zhang, C., 2016. An unexpected disruption of the atmospheric quasi-biennial oscillation. *Science* 353, 1424–1427.

Pascoe, C.L., Gray, L.J., Crooks, S.A., Jukes, M.N., Baldwin, M.P., 2005. The quasi-biennial oscillation: Analysis using ERA-40 data. *Journal of Geophysical Research: Atmospheres* 110.

Porco, C.C., West, R.A., McEwen, A., Del Genio, A.D., Ingersoll, A.P., Thomas, P., Squyres, S., Dones, L., Murray, C.D., Johnson, T.V., et al., 2003. Cassini imaging of Jupiter’s atmosphere, satellites, and rings. *Science* 299, 1541–1547.

Rodgers, C.D., 2000. *Inverse Methods for Atmospheric Sounding: Theory and Practice*. World Scientific.

Rogers, J., 2017. Jupiter in 2016-2017. British Astronomical Association URL: <https://britastro.org/node/8103>.

Rothman, L.S., Jacquemart, D., Barbe, A., Benner, D.C., Birk, M., Brown, L., Carleer, M., Chackerian, C., Chance, K., Coudert, L., et al., 2005. The HITRAN 2004 molecular spectroscopic database. *Journal of Quantitative Spectroscopy and Radiative Transfer* 96, 139–204.

Sánchez-Lavega, A., Orton, G., Hueso, R., García-Melendo, E., Pérez-Hoyos, S., Simon-Miller, A., Rojas, J., Gómez, J., Yanamandra-Fisher, P., Fletcher, L., et al., 2008. Depth of a strong jovian jet from a planetary-scale disturbance driven by storms. *Nature* 451, 437.

Sánchez-Lavega, A., Rogers, J.H., Orton, G., García-Melendo, E., Legarreta, J., Colas, F., Dauvergne, J., Hueso, R., Rojas, J.F., Pérez-Hoyos, S., et al., 2017. A planetary-scale disturbance in the most intense jovian atmospheric jet from JunoCam and ground-based observations. *Geophysical Research Letters* 44, 4679–4686.

Simon-Miller, A.A., Conrath, B.J., Gierasch, P.J., Orton, G.S., Achterberg, R.K., Flasar, F.M., Fisher, B.M., 2006. Jupiter’s atmospheric temperatures: from Voyager IRIS to Cassini CIRS. *Icarus* 180, 98–112.

Wong, M.H., Simon, A.A., Tollefson, J.W., de Pater, I., Barnett, M.N., Hsu, A.I., Stephens, A.W., Orton, G.S., Fleming, S.W., Goullaud, C., et al., 2020. High-resolution UV/Optical/IR Imaging of Jupiter in 2016–2019. *The Astrophysical Journal Supplement Series* 247, 58.